Ordered mesoporous silica nanoparticles with and without embedded iron oxide nanoparticles: structure evolution during synthesis

Teeraporn Suteewong,[a] Hiroaki Sai,[a] Jinwoo Lee,[b] Michelle Bradbury,[c] Taeghwan Hyeon,[d] Sol M. Gruner[ef] and Ulrich Wiesner*[a]

This work reports on the structural evolution during room temperature synthesis of hexagonally ordered mesoporous silica nanoparticles with and without embedded iron oxide particles. Oleic acid-capped iron oxide nanoparticles are synthesized and transferred to an aqueous phase using the cationic surfactant, hexadecyltrimethylammonium bromide (CTAB). MCM-41 type silica and composite nanoparticles are fabricated *via* sol–gel synthesis. Aliquots are taken from the solution during synthesis to capture the particle formation process. Transmission Electron Microscopy (TEM) and Small Angle X-ray Scattering (SAXS) reveal a transition from a disordered to an ordered structure in both synthesis systems. Along with the evolution of structure, iron oxide nanoparticles acting as seeds at the early stages are relocated from the particle centers to the edges. Nitrogen sorption measurements for iron oxide-embedded mesoporous nanoparticles indicate surface areas as high as for the mesoporous silica nanoparticles without iron oxide.

Introduction

Since the pioneering work by Stöber *et al.*, silica nanoparticles have been explored as candidates for a variety of applications including photonics and biomedicine.[1,2] Nano-sized silica materials provide not only excellent intrinsic properties, such as low toxicity, excellent chemical stability and versatile functionalization chemistry, but also have the capability of being platforms for, or being integrated with, other nanomaterials.[3] The aforementioned characteristics have led to the development of multifunctional nanocomposites, in which properties of individual components are combined to create new features including drug delivery systems and lasing.[4,5] Silica-based nanomaterials with new functionalities have been continuously developed. One example is one-dimensional hexagonally ordered mesoporous silica, known as MCM-41.[6–8] This material possesses uniform and tunable pore size, functionalizable surfaces, high specific surface area and large pore volume suitable for a variety of potential applications.[9–15] By modification of the Stöber method, Grun *et al.* reported the first synthesis of micrometre-size MCM-41-type particles.[16] Since then, nano-sized MCM-41 materials have been explored for biological applications.

Combining mesoporous silica with metals and metal oxides results in hybrid mesoporous silica nanoparticles with combinations of properties. Such hybrids could be used in applications, such as drug delivery, MRI and catalysis.[3,11–14,17–22] A hexagonal pore arrangement could facilitate the use of these nano-sized materials to the desired purposes. However, generation and preservation of such periodic silica structure during synthesis and processing is always a challenge. There have been many attempts to incorporate inorganic nanoparticles into the siliceous matrix without loss of the ordered structure. Back filtration of metal salt solutions into the pre-formed mesoporous materials and subsequent *in situ* formation of metal particles have been applied to synthesize metal particle-embedded mesoporous silica composites.[17] Nooney and co-workers successfully grew a mesoporous silica shell onto silica-coated gold nanoparticles.[23,24] Similarly, tumbler-like ordered mesoporous silica nanoparticles were synthesized at 50 °C in the presence of silica-coated magnetic nanoparticles.[18,21] Recently, one-pot syntheses of magnetic core-containing silica nanospheres with ordered periodic mesostructure at elevated temperature (80 °C and below 65 °C, respectively) were reported.[14,25,26] In order to fabricate such hierarchical hybrid materials with optimal structure control, it is of interest to understand the formation mechanism. Indeed, several formation mechanisms have been proposed based on the structures of the final products.[14,24,26] What has been mostly lacking in the literature, however, is a systematic study of the formation mechanism with identification of early, intermediate and final stages of materials structure.

The present work reports on room temperature synthesis of magnetic iron oxide nanoparticle-containing MCM-41-type nanoparticles. The goal is to elucidate the formation mechanism to allow control of the location of the iron oxide nanoparticles within the siliceous particle matrix. To this end, magnetite particles were synthesized using a thermal decomposition method.[27] The resulting oleic acid-capped inorganic

[a] Department of Materials Science and Engineering, Cornell University, 330 Bard Hall, Ithaca, NY, 14853, USA. E-mail: ubw1@cornell.edu; Fax: +1 607 255 2365

[b] Department of Chemical Engineering and School of Environmental Science and Engineering, Pohang University of Science and Engineering, Pohang, Republic of Korea

[c] Department of Radiology, Memorial Sloan-Kettering Cancer Centre, 1275 York Avenue, New York, NY, 10065, USA

[d] Center for Nanocrystalline Materials and School of Chemical and Biological Engineering, Seoul National University, Seoul, Republic of Korea

[e] Department of Physics, Cornell University, Ithaca, NY, 14853, USA

[f] Cornell High Energy Synchrotron Source (CHESS), Cornell University, Ithaca, NY, 14853, USA

This journal is © The Royal Society of Chemistry 2010

J. Mater. Chem., 2010, 20, 7807–7814 | 7807

nanoparticles were transferred into an aqueous phase using a cationic surfactant, hexadecyltrimethylammonium bromide (CTAB).[12] The sol–gel silica reaction was performed in the presence of the CTAB-stabilized iron oxide nanoparticles. The dilution/neutralization method reported by Mann and co-workers was employed to lower the reaction rates and associated aggregation.[28,29] Aliquots were taken at different time points for which the reaction was halted by the addition of hydrochloric acid. The structures at different reaction times were studied using Transmission Electron Microscopy (TEM) and Small Angle X-ray Scattering (SAXS) and compared to results of the synthesis of MCM-41-type nanoparticles without embedded iron oxide nanoparticles. Surface area and pore size were inferred from nitrogen adsorption/desorption measurements.

Experimental

Chemicals

Hexadecyltrimethylammonium bromide (approx. 99%), ethyl acetate (ACS grade), tetraethyl orthosilicate (TEOS, $\geq$99%, GC), ammonium hydroxide (29%), acetic acid (glacial), hydrochloric acid (36.5–38%), ethanol (absolute, anhydrous), deionized water (Milli-Q, 18.2 MΩ-cm), chloroform (AR grade), 1-octadecene (AR grade), iron(III) oxide (FeO(OH)) (hydrated, 30–50 mesh), oleic acid (technical grade, 90%) and acetone (AR grade) were used as obtained without further purification.

Synthesis of magnetic nanoparticles

Iron oxide nanoparticles (8–9 nm) were synthesized as reported in the literature.[27] FeO(OH) (0.356 g) was mixed with oleic acid (4.52 g) and 1-octadecene (10 mL) in a three-necked round bottom flask. While stirring, nitrogen gas was purged through the mixture for 10 min before heating to 320 °C for 1 h. After cooling to room temperature, the as-made nanoparticles were cleaned by the addition of acetone and separated by centrifugation. After removal of the supernatant, the particles were re-dispersed in hexane and the washing procedure was repeated two more times. The particles were suspended in chloroform for the next step.

Phase transfer of magnetic particles to aqueous phase

Magnetic nanoparticles (15 mg in 0.5 mL of chloroform) were added to aqueous CTAB solution (5 mL, 54.8 mM). The mixture was stirred until a homogeneous microemulsion was formed. The solution was then transferred to a pre-heated oil bath at 70 °C for 10 min to evaporate the chloroform as well as to induce the interaction between the hydrophobic chains of the two surfactants.

Synthesis of mesoporous silica nanoparticles incorporating magnetic nanoparticles

The fabrication of iron oxide–silica nanoparticle composites was modified from Kim et al. and Fowler et al.[12,28] As-made CTAB-stabilized magnetic nanoparticles solution (0.5 mL) was diluted in water (10 mL), followed by the addition of ethyl acetate (0.088 mL). NH$_4$OH (0.27 mL) and TEOS (50 μL) were subsequently added and the solution was stirred for 5 minutes. Then, water (3.69 mL) was added into the reaction, which proceeded for another 10 minutes. Aliquots were taken from the reaction mixture every

minute and neutralized by adding 2 M HCl. The resulting material was cleaned by centrifugation using water and ethanol. To remove the surfactant templates, in the last washing, particles were redispersed in an ethanol/acetic acid (glacial) mixture (95/5, v/v) and the mixture was stirred for 30 minutes. Centrifugation in water and ethanol was employed in the cleaning step.

Synthesis of mesoporous silica nanoparticles without magnetic nanoparticles
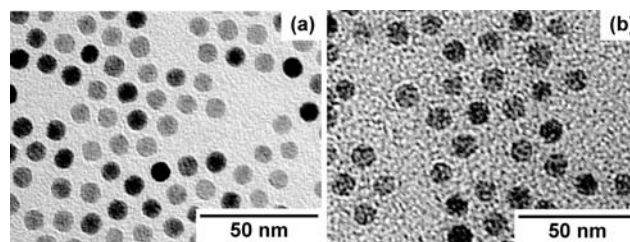
For comparison, mesoporous silica nanoparticles were synthesized in the absence of CTAB-stabilized magnetic nanoparticles. CTAB solution (0.5 mL, 54.8 mM) was added into water (10 mL). The subsequent steps were identical to what has been described in the foregoing synthesis of magnetic nanoparticle-embedded mesoporous silica nanoparticles.

Characterization

Transmission Electron Microscopy (TEM) images were obtained with an FEI Tecnai T12 Spirit microscope operated at an acceleration voltage of 120 kV. Particle size distributions were obtained by averaging over approximately 30 (short aging times) to 100 (longer aging times) particles. The standard deviation is reflected in error bars in Fig. 5. Small-Angle X-ray Scattering (SAXS) patterns of samples after surfactant template removal in dry and wet forms were obtained on a home-built beamline as previously described,[30] as well as on the G1 beamline in Cornell High Energy Synchrotron Source (CHESS). Nitrogen physisorption isotherms of dried samples were obtained with a Micromeritics ASAP2020 physisorption instrument.

Results

Integrating inorganic nanoparticles into ordered mesoporous materials without disrupting the ordered structure of the matrix is a challenge. Only a few reports on one-step synthesis processes exist.[14,23–25] Silica condensation in the presence of seed particles normally yields a core/shell morphology, i.e., pre-formed particle cores with a secondary material shell. In the case of MCM-41 type mesoporous silica nanoparticles incorporating iron oxide nanoparticles, it is of interest to investigate the evolution of structure at different reaction times. To this end, we synthesized magnetic nanoparticles using thermal decomposition, yielding monodisperse particle sizes around 8–9 nm (Fig. 1(a)). As-synthesized iron oxide particles were capped with oleic acid making them soluble in an organic solvent. Fig. 2 shows a schematic representing the transfer of oleic acid-capped iron oxide

Fig. 1 TEM of (a) oleic acid-capped iron oxide nanoparticles and (b) CTAB-coated iron oxide nanoparticles.
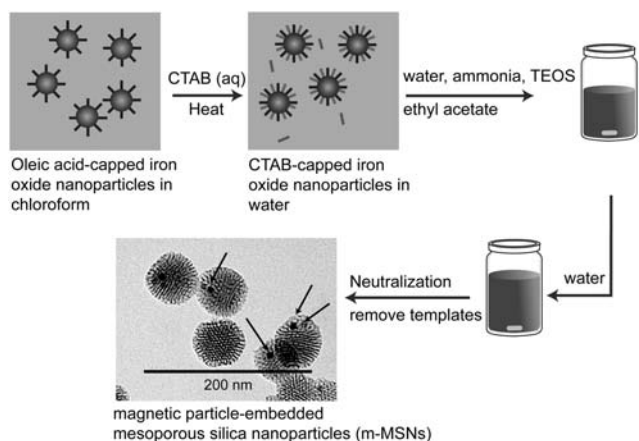
Fig. 2 Synthesis scheme for magnetic particle-containing mesoporous silica nanoparticles (m-MSNs). Arrows indicate iron oxide nanoparticles incorporated.

from chloroform to an aqueous solution of CTAB.[12] Upon heating, the organic solvent evaporated and particles were transferred to an aqueous phase driven by the van der Waals interactions between the hydrophobic chains of adsorbed ligands on the particle surface and of CTAB, leading to the formation of bilayer structures with quaternary ammonium groups pointing

outwards.[14] Resulting particles (Fig. 1(b)) were diluted further before the addition of the silica precursor TEOS. A sol–gel reaction proceeding in the presence of CTAB-modified magnetic nanocrystals, with subsequent removal of the surfactant templates yielded highly ordered mesoporous silica nanoparticles with magnetic particles embedded in the matrix, referred to as m-MSNs. The size of the m-MSNs in Fig. 2 is 62 ± 10 nm and the iron oxide in the electron micrographs appears to be predominately near the outer particle surface rather than in the particle center. To the best of our knowledge, this is the first report on room temperature and short time scale (15 minutes) synthesis of magnetic nanoparticles embedded in highly ordered mesoporous silica nanoparticles.

In the present study, after adding TEOS, the mixture was stirred for 5 minutes (mixing time). Then, additional water was added into the system and the reaction proceeded for another 10 minutes (aging time). During aging, aliquots were taken every minute and neutralized to halt the ongoing chemical processes. The addition of water after the first 5 minutes causes a decrease in the pH of the system, which results in slowing of silica hydrolysis but accelerates the silica condensation.[28,29] Templates were subsequently removed using acid extraction (see Experimental) and air dried. TEM images of m-MSNs at different aging times are shown in Fig. 3. An interesting structural evolution from disordered to ordered silica as a function of the aging time from
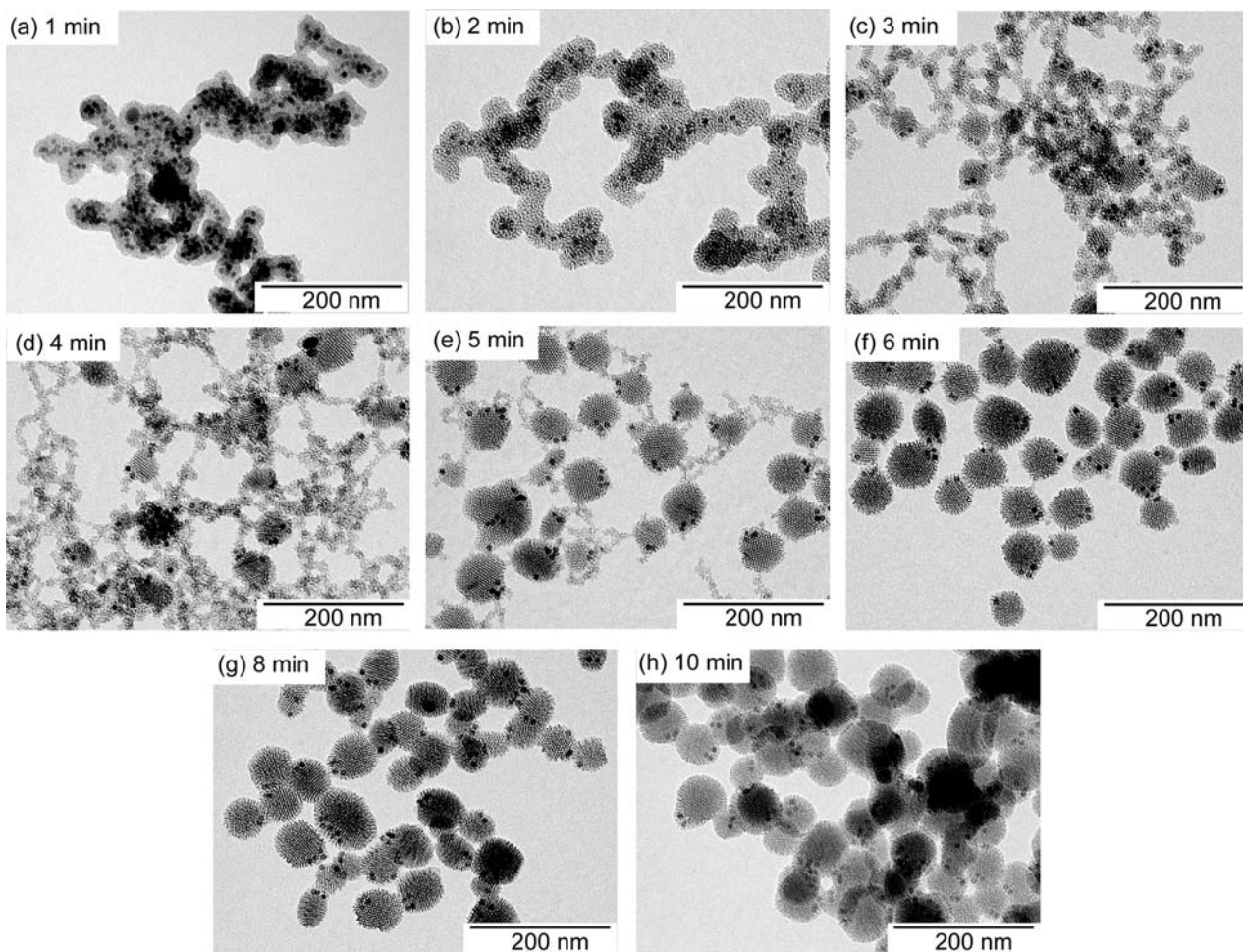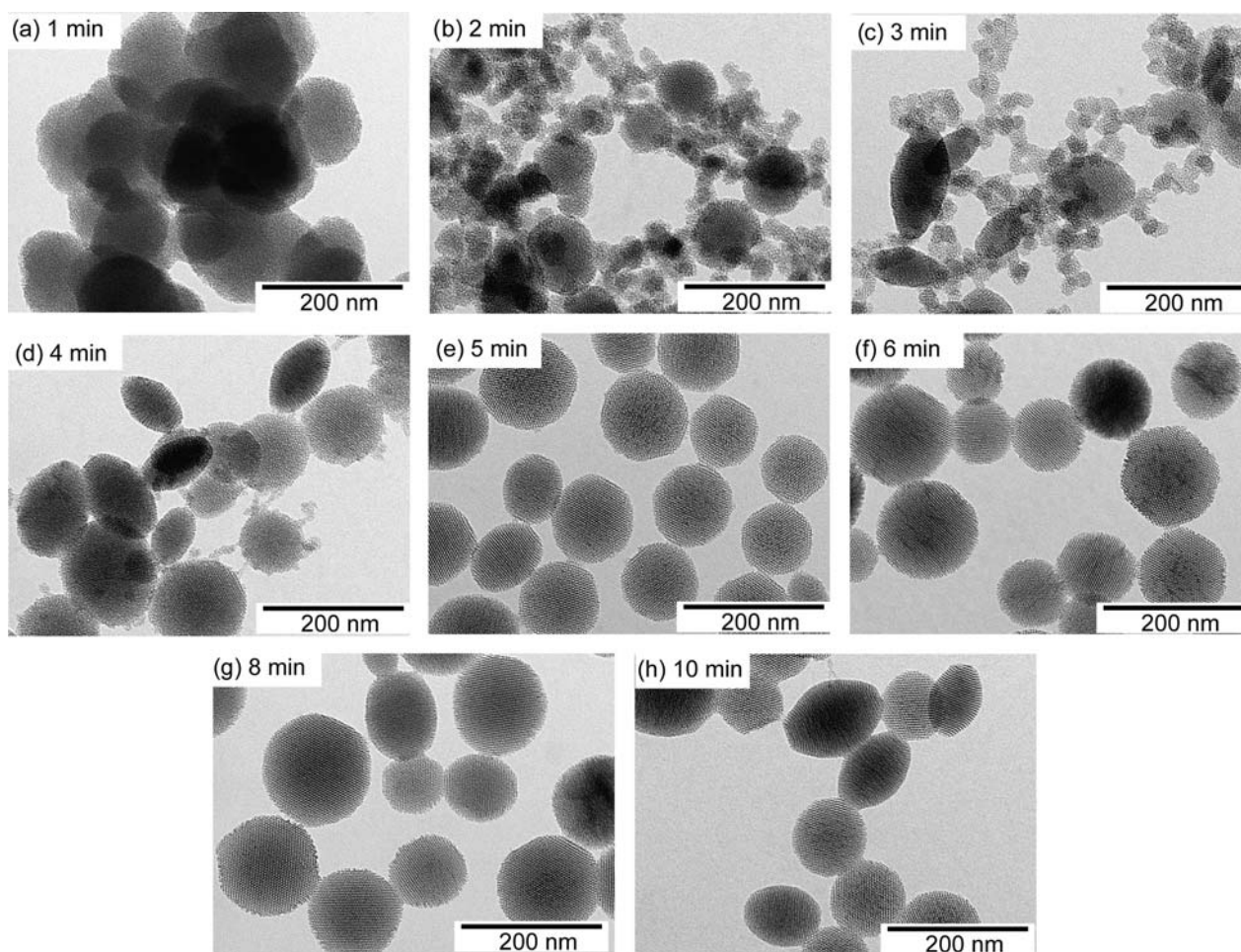

Fig. 3 TEM of m-MSNs captured at different aging times from 1 to 10 minutes (a–h).

1 to 10 min is observed in these images including a change in location of the iron oxide particles from the center to the outer edge of the siliceous matrix. At the early aging stage (1–2 minutes), a core/shell type morphology with iron oxide cores and porous silica shells is found (Fig. 3(a) and (b)), similar to what has been previously reported.[14] TEM images suggest that the iron oxide nanoparticles are all distributed within a disordered silica shell. The particles are about 42 ± 5 nm in size. At aging time 3 minutes (Fig. 3(c)), the inorganic particles are no longer located in the middle of the silica matrix, but are relocating to the edges. The structure of the silica matrix itself is also changing, *i.e.*, order is developing and, besides the primary particles, small secondary clusters of porous silica are forming. These clusters decrease in number when the reaction time increases (Fig. 3(d) and (e)) and disappear after about 6 minutes of aging time (Fig. 3(f)). Beyond 6 minutes, the morphology of the nanoparticle composites does not change significantly. After that time, highly ordered MCM-41-type nanoparticles containing iron oxide particles at their edges are obtained that are about 63 ± 9 nm in size.

As a control, mesoporous silica particles without magnetic particle seeds (referred to as b-MSNs) were synthesized according to the protocol described in the Experimental section. TEM images of b-MSNs at different aging times are shown in Fig. 4. Overall the structural evolution is similar to that in Fig. 3, albeit

exhibiting different particle sizes and kinetics. An accelerated disorder-to-order transition is observed, relative to the m-MSNs case. At an aging time of 1 minute, agglomerates of porous silica particles are seen. Although difficult to precisely determine, the size of the primary particles is of order 100 nm, *i.e.*, significantly larger than the primary particles obtained in the presence of iron oxide. The development of order starts at 2 minutes and can be clearly discerned at an aging time of 3 minutes (Fig. 4(c)). At the 2 minute time point, secondary and loosely packed porous silica particles, roughly 20 nm in diameter, appear in TEM (Fig. 4(b)). They disappear over the next 2 minutes and are absent in the image representing the time point of 5 minutes (Fig. 4(e)). Particle size as well as structural order increases with increasing aging time. No significant changes are seen beyond about 5 minutes. The size of the final particles in Fig. 4 is 117 ± 23 nm, *i.e.*, significantly larger than that of the iron oxide containing particles in Fig. 3.

Particle size and size distributions of m-MSNs and b-MSNs at different aging times measured from TEM images are shown in Fig. 5. Data at an aging time of 1 minute are excluded due to the aggregation of particles, making analysis difficult. Particle size increases in both cases with increasing aging time for about the first 7 minutes, with no significant changes after that. From this plot, it is evident (i) that particles with iron oxide seeds are

**Fig. 4** TEM of b-MSNs captured at different aging times from 1 to 10 minutes (a–h).
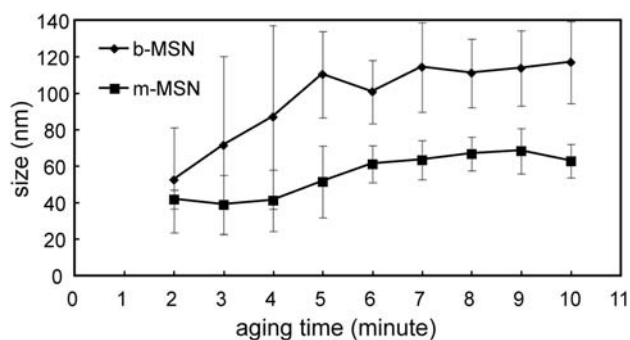
Fig. 5 Particle sizes and size distributions of m-MSNs and b-MSNs at different aging times as obtained from TEM data analysis.

Fig. 6 SAXS patterns of (a) b-MSN samples in vacuum dried form and suspensions (aqueous native solution, cleaned particles in ethanol before and after removal of CTAB) at an aging time of 10 minutes and SAXS patterns of dry CTAB-removed samples of (b) m-MSNs and (c) b-MSNs at different aging times from 1 to 10 minutes.

smaller at any stage as compared to the control particles without iron oxide, (ii) that particle growth is accelerated for b-MSNs relative to m-MSNs, and (iii) that particle size distributions are larger in the case of b-MSNs throughout the formation process as obtained from analysis of TEM images.

In order to better characterize the structural order inside the particles, Small-Angle X-ray Scattering (SAXS) was used. Radially integrated scattering intensity profiles of particles in native solution (no treatment performed after neutralization), cleaned as-made particles in ethanol (before removing CTAB) and CTAB-removed particles in ethanol are shown in Fig. 6(a). They were investigated in order to exclude significant structural transitions upon different processing steps. All solution patterns were taken at an aging time of 10 minutes. According to the SAXS patterns shown in Fig. 6(a), there is no structural transition upon template removal. Compared to solution samples, however, SAXS reflections of dried samples taken at 10 minute aging times slightly shift to higher q values. For example, the first order peak shifts from 1.66 nm^{-1} in wet samples to 1.76 nm^{-1} in dried samples, where q denotes the scattering vector and is defined as $q = (4\pi \sin \theta)/\lambda$ with a scattering angle 2θ and the X-ray wavelength $\lambda = 1.54$ Å. This shift likely results from a contraction induced by further silica condensation upon drying. While scattering intensities from the suspensions are smaller than those from dried samples aside from peak shift, significant structural transitions were not observed upon drying. We therefore subsequently consider and discuss results only on the dried samples.

The structural evolution of nanoscale order during the particle formation in the 10 minute timeframe is studied for both m-MSN and b-MSN samples. A set of peaks at $q = 1.7$, 3.0, 3.5 and 4.6 nm^{-1} is observed. These reflections are consistent with the (10), (11), (20) and (21) peaks of a hexagonally packed cylindrical structure with an inter-channel distance of 4.2 nm. A broader set of peaks that initially appears at $q = 1.5$ and 3.0 nm^{-1} for b-MSNs and at $q = 1.3$ and 2.6 nm^{-1} for m-MSNs diminishes as the hexagonal peaks grow stronger. Both materials develop a more defined pattern characteristic of MCM-41 as time progresses. In the case of m-MSNs, a peak at $q = 1.3$ nm^{-1} and a broad hump at 2.6 nm^{-1} can be observed from 1 to 4 minutes of aging time. At the 3 and 4 minute time points, the peak at lower q broadens toward higher q values. After that, starting from an aging time of 5 minutes, a more pronounced peak evolves at 1.7 nm^{-1}. As time progresses, additional peaks at $q = 3$ and 3.5 nm^{-1} are appearing, while after about 8 minutes of aging time,
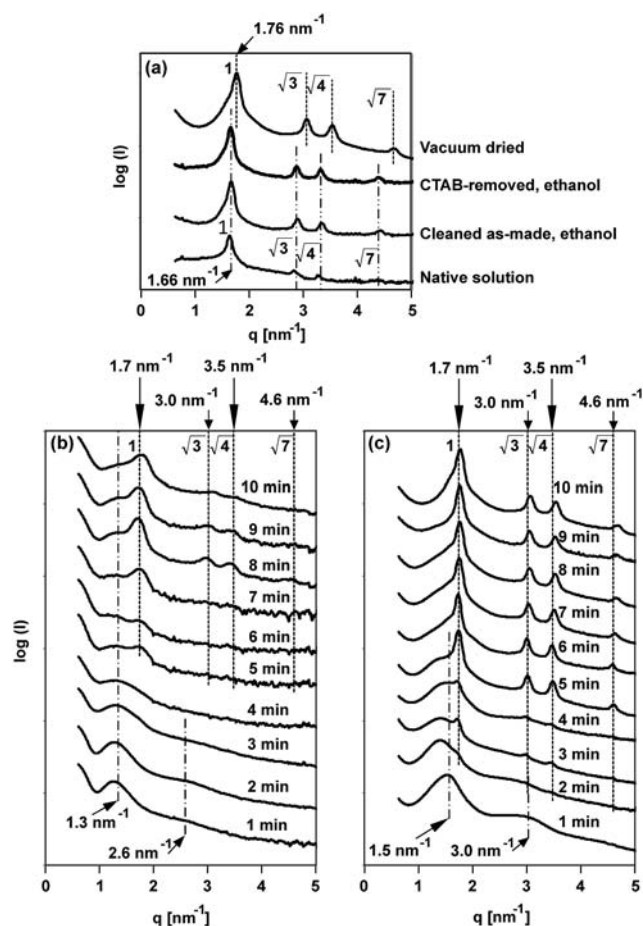
no significant further changes are observed. Similar trends are found in the kinetics study of b-MSN samples. However, a clear onset of hexagonal order is already observed at about 2 minute aging time, i.e., significantly earlier than for m-MSNs. The biggest structural changes here occur between about 2 and 5 minutes, whereas after about 6 minutes, there are no significant further changes in the SAXS patterns of b-MSNs.

The N_2 sorption isotherms of MSNs with and without magnetic particles are shown in Fig. 7. Both data sets exhibit type IV isotherms, without hysteresis loops, meaning that all pores are accessible. The pore size of m-MSNs as derived from the Barrett–Joyner–Halenda (BJH) analysis is almost unchanged over that of b-MSNs: 2.74 and 2.70 nm for m-MSNs and b-MSNs, respectively.[31,32] The presence of magnetic particles incorporated into the siliceous matrix slightly affected the Brunner–Emmett–Teller (BET) specific surface area of MSNs, however, which was 893 m^2 g^{-1} for m-MSNs and 1240 m^2 g^{-1} for b-MSNs.

Discussion

In the past, multiple studies reported on the formation mechanisms of MCM-41 type materials, especially in the bulk.[8,33–35] No single mechanism has been fully agreed to, however,[9] because the

This journal is © The Royal Society of Chemistry 2010

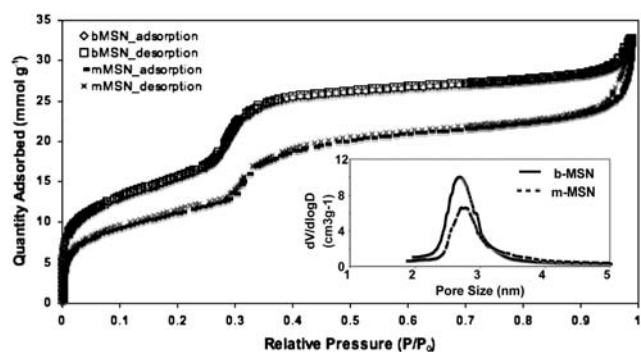*J. Mater. Chem.*, 2010, **20**, 7807–7814 | 7811

Fig. 7 N$_2$ sorption isotherms of b-MSNs and m-MSNs after 10 minutes of aging time. Inset: pore size distributions as obtained from adsorption measurements (V = pore volume and D = pore size).

synthesis conditions typically change from one study to another, including temperature, catalyst, reaction time, solvent, pH, type of silica source and concentration of reactants. Based on this body of work, the synthesis and applications of ordered MSNs embedded iron oxide nanoparticles have been described. Less time has been devoted to elucidating their formation mechanisms. To this end, herein, the formation of ordered MSNs containing magnetic nanoparticles is elucidated based on TEM and SAXS measurements of particles and controls at different time points. The syntheses of inorganic nanoparticle-containing MSNs with and without ordered structure have been reported.[12,14,21,24–26,36]

Less attention has been paid to the correlation between the location of the magnetic particles and the structure evolution of the mesoporous matrix. Nooney *et al.* reported the synthesis of mesoporous silica/gold composite particles by growing a mesoporous silica layer on pre-existing nuclei, *i.e.*, silica-coated gold nanoparticles.[24] Both disordered and ordered mesoporous silica/gold particles were found depending on the given synthesis conditions: if water was the only solvent, hexagonally-shaped ordered porous silica composites were observed, in which the gold seeds were located close to the particle edges. Under such conditions, elongated CTAB micelle–silica aggregates are formed preferring a directional aggregation to form an ordered structure on the existing silica-coated gold nanoparticles. If alcohol was used as co-solvent, however, micelles had smaller aspect ratios and their packing was disturbed yielding a disordered porous silica shell around center-located gold seeds. Zhang and co-workers reported on the fabrication of magnetic core/ordered mesoporous silica shell nanospheres.[14] Stearic acid-capped magnetic particles were transferred to aqueous phase using different alkyltrimethylammonium bromide surfactant chain lengths (C14–C18), prior to the synthesis of porous silica shells at 80 °C for 2 h. TEM images showed that iron oxide nanocrystals were well distributed in the center of the particles. Cationic surfactant-modified iron oxide particles acted as seeds for the packing and self-assembly of silica–surfactant complexes.

What both cases have in common is the incorporation of inorganic particles into the structurally ordered matrix. However, different inorganic particle locations and silica particle shapes were observed. The deduction of the particle formation mechanism based on the shape and morphology of the final materials is difficult, however. What happens during particle growth of such composites may help elucidate key steps in the formation processes leading to better control. To this end, here, we presented a kinetics study of the formation of magnetic nanoparticle-containing MCM-41 silica nanoparticles by tracking the reaction at different time points.

For simplicity, the key observations are divided into two periods: *i.e.*, the early stage (before an ordered structure is developed) and the ordering/restructuring stage, where the evolution of hexagonally arrayed cylinders is observed. During the early stage, comparing particle sizes and size distributions from TEM data analysis shown in Fig. 5, initial particle sizes (aging time = 2 minutes) are significantly smaller when iron oxide seeds are present, *i.e.*, about 42 ± 5 nm for m-MSNs and about 52 ± 29 nm for b-MSNs. The size distribution is also smaller when magnetic particles are present. The location of magnetic particles initially (1–2 minutes of aging time) is in the center of the silica nanoparticles, see Fig. 3(a) and (b)). These observations suggest that the magnetic nanoparticles may act as seeds for the growth of more homogeneously sized mesoporous silica particles. This is corroborated by additional experiments (data not shown) in which we decreased the amount of seed particles resulting in larger m-MSN size. During the second stage, *i.e.*, during the development of hexagonal structure (Fig. 3(c)–(h)), the disorder-to-order transition of the silica matrix is retarded by the presence of magnetic nanoparticles. Upon silica ordering, the magnetic nanoparticles are relocated to the boundaries of the ordered domains, a process that is typical for crystallization in the presence of impurities.[37] These results imply that magnetic nanoparticles act as impurities, which delay the crystallization process and end up at the grain boundaries. The other noticeable feature in Fig. 3(c)–(f) is the existence of small secondary porous silica particles formed during the ordering stage. We suggest that this secondary nucleation and growth burst are associated with the second addition of water. While the primary particles grow, the secondary particles decrease in number and disappear, suggesting Ostwald ripening.

Fig. 8 is an illustration of the observed formation mechanism of m-MSNs. This cartoon is divided into 3 parts: Part I shows the stepwise addition of all synthesis components, the middle part describes the mixing step taking place for 5 minutes after the addition of TEOS, and the last part describes the aging step, for which the kinetics study was conducted. The addition of TEOS initiates Part II. Phase separation of small TEOS droplets occurs from the aqueous phase due to its immiscibility with water. This phenomenon suggests that dissolution time is the rate limiting step.[24] TEOS molecules are hydrolyzed at the TEOS/water droplet interface generating ethanol as a by-product. This gradually changes the polarity of the system increasing the solubility of TEOS. Condensation between hydrolyzed TEOS molecules happens along with the electrostatic interaction with surfactant-stabilized inorganic particles, free surfactant molecules and surfactant micelles leading to the formation of magnetic core/porous silica shell particles as observed in Fig. 3(a) and (b).[14] This process is seeded by the small magnetic nanoparticles. Seeding leads to smaller overall particle size and smaller particle size distributions as compared to the unseeded process. Water added at the end of the mixing step induces a sudden change in TEOS solubility and initiates Part III. This causes a secondary nucleation burst, yielding the formation of
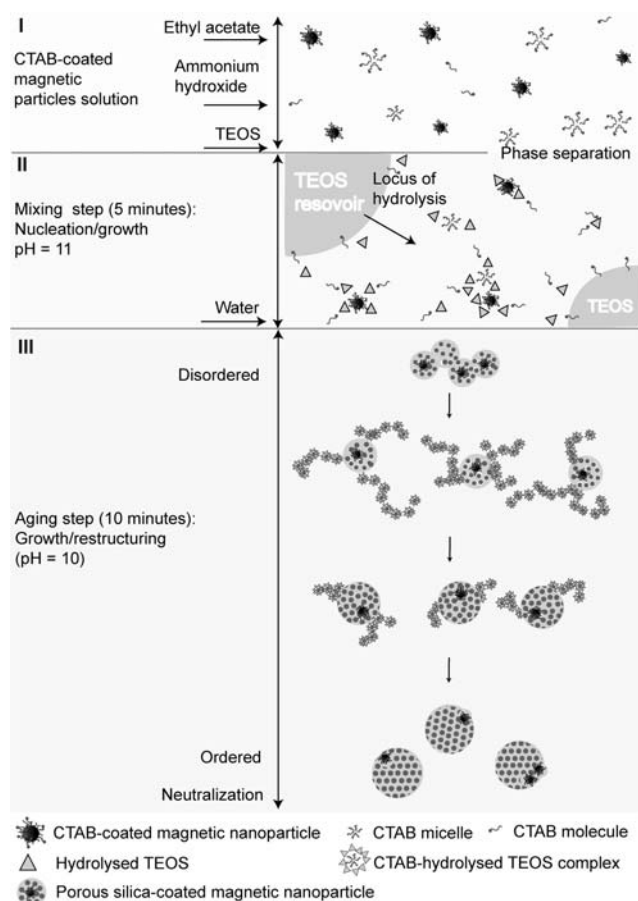
Fig. 8 Proposed formation mechanism of m-MSNs.

small secondary silica nanoparticles. These later-formed nanoparticles are consumed by the growing primary nanocomposites in an Oswald ripening-type process.

Lowering the solution pH is expected to be an important factor in restructuring silica into highly hexagonally ordered structures.[10] Two parameters affecting pH in this study are ethyl acetate and water added after the mixing step. Ethyl acetate is hydrolyzed and gradually decreases the pH of the solution.[10] So does the addition of extra water. From TEM and SAXS results, the presence of magnetic nanoparticles influences the structural change in the siliceous matrix. Studies on the capture of inclusions during crystallization processes from melts and solutions have been described.[37,38] Temperature, growth rate, size of inclusions/foreign particles and surface interactions between the growth front and foreign particles are all known to affect crystallization.[37] For instance, if the growth rate is high enough, particles will be captured inside crystals. It is also possible that particles will be repelled from the growing crystal front if the surface compatibility is poor. Even though the exact determination of aforementioned parameters is beyond the scope of this study, the general concept of incorporation of particles into growing crystals can be applied to explain our observations. If the disorder-to-order structure transition is considered as a crystallization process, the front of the ordered region could be thought of as the front of a growing crystal, which repels the foreign particle away to the grain boundaries while retarding crystallization (see Fig. 6). Completion of the ordering

(crystallization) leads to particles that all have the iron oxide at the edges of particles, see Fig. 3(f)–(h).

Conclusion

Mesoporous silica nanoparticles incorporating magnetic nanoparticles have been synthesized at room temperature through a sol–gel synthesis. Capturing the reaction at different time points during the synthesis has helped to elucidate the formation mechanism. TEM and SAXS data show the structure evolution with primary and secondary nucleation steps, from disordered to ordered silica as well as show a change in location of iron oxide particle inclusions from the center to the edge of the silica matrix. Comparison to synthesis of mesoporous silica nanoparticles in the absence of iron oxide reveals that the iron oxide nanoparticles seed the silica formation leading to much smaller particles with lower size dispersion. The iron oxide inclusions further retard the transition from disordered to ordered silica which can be understood by considering the ordering process as a crystallization and the iron oxide as an impurity which is relocated towards grain boundaries (particle edges).

Disclaimer

Acknowledgements

References

1 W. Stöber, A. Fink and E. Bohn, *J. Colloid Interface Sci.*, 1968, **26**, 62–69.
2 A. Burns, H. Ow and U. Wiesner, *Chem. Soc. Rev.*, 2006, **35**, 1028–1042.
3 Y. Piao, A. Burns, J. Kim, U. Wiesner and T. Hyeon, *Adv. Funct. Mater.*, 2008, **18**, 3745–3758.
4 S. H. Hu, D. M. Liu, W. L. Tung, C. F. Liao and S. Y. Chen, *Adv. Funct. Mater.*, 2008, **18**, 2946–2955.
5 M. A. Noginov, G. Zhu, A. M. Belgrave, R. Bakker, V. M. Shalaev, E. E. Narimanov, S. Stout, E. Herz, T. Suteewong and U. Wiesner, *Nature*, 2009, **460**, 1110–1113.

6 T. Yanagisawa, T. Shimizu, K. Kuroda and C. Kato, *Bull. Chem. Soc. Jpn.*, 1990, **63**, 988–992.

7 J. S. Beck, J. C. Vartuli, W. J. Roth, M. E. Leonowicz, C. T. Kresge, K. D. Schmitt, C. T. W. Chu, D. H. Olson, E. W. Sheppard, S. B. McCullen, J. B. Higgins and J. L. Schlenker, *J. Am. Chem. Soc.*, 1992, **114**, 10834–10843.

8 C. T. Kresge, M. E. Leonowicz, W. J. Roth, J. C. Vartuli and J. S. Beck, *Nature*, 1992, **359**, 710–712.

9 J. Y. Ying, C. P. Mehnert and M. S. Wong, *Angew. Chem., Int. Ed.*, 1999, **38**, 56–77.

10 T. Linssen, K. Cassiers, P. Cool and E. F. Vansant, *Adv. Colloid Interface Sci.*, 2003, **103**, 121–147.

11 B. G. Trewyn, C. M. Whitman and V. S. Y. Lin, *Nano Lett.*, 2004, **4**, 2139–2143.

12 J. Kim, J. E. Lee, J. Lee, J. H. Yu, B. C. Kim, K. An, Y. Hwang, C. H. Shin, J. G. Park and T. Hyeon, *J. Am. Chem. Soc.*, 2006, **128**, 688–689.

13 J. Kim, H. S. Kim, N. Lee, T. Kim, H. Kim, T. Yu, I. C. Song, W. K. Moon and T. Hyeon, *Angew. Chem., Int. Ed.*, 2008, **47**, 8438–8441.

14 L. Zhang, S. Z. Qiao, Y. G. Jin, H. G. Yang, S. Budihartono, F. Stahr, Z. F. Yan, X. L. Wang, Z. P. Hao and G. Q. Lu, *Adv. Funct. Mater.*, 2008, **18**, 3203–3212.

15 K. Moller and T. Bein, *Chem. Mater.*, 1998, **10**, 2950–2963.

16 M. Grun, I. Lauer and K. K. Unger, *Adv. Mater.*, 1997, **9**, 254–257.

17 M. Arruebo, M. Galan, N. Navascues, C. Tellez, C. Marquina, M. R. Ibarra and J. Santamaria, *Chem. Mater.*, 2006, **18**, 1911–1919.

18 N. Gov, I. Borukhov and D. Goldfarb, *Langmuir*, 2006, **22**, 605–614.

19 J. Gu, W. Fan, A. Shimojima and T. Okubo, *Small*, 2007, **3**, 1740–1744.

20 I. I. Slowing, B. G. Trewyn and V. S. Y. Lin, *J. Am. Chem. Soc.*, 2007, **129**, 8845–8849.

21 H. M. Liu, S. H. Wu, C. W. Lu, M. Yao, J. K. Hsiao, Y. Hung, Y. S. Lin, C. Y. Mou, C. S. Yang, D. M. Huang and Y. C. Chen, *Small*, 2008, **4**, 619–626.

22 J. E. Lee, N. Lee, H. Kim, J. Kim, S. H. Choi, J. H. Kim, T. Kim, I. C. Song, S. P. Park, W. K. Moon and T. Hyeon, *J. Am. Chem. Soc.*, 2010, **132**, 552–557.

23 R. I. Nooney, D. Thirunavukkarasu, Y. M. Chen, R. Josephs and A. E. Ostafin, *Chem. Mater.*, 2002, **14**, 4721–4728.

24 R. I. Nooney, D. Thirunavukkarasu, Y. M. Chen, R. Josephs and A. E. Ostafin, *Langmuir*, 2003, **19**, 7628–7637.

25 Y. S. Lin and C. L. Haynes, *Chem. Mater.*, 2009, **21**, 3979–3986.

26 M. Liong, J. Lu, M. Kovochich, T. Xia, S. G. Ruehm, A. E. Nel, F. Tamanoi and J. I. Zink, *ACS Nano*, 2008, **2**, 889–896.

27 W. W. Yu, J. C. Falkner, C. T. Yavuz and V. L. Colvin, *Chem. Commun.*, 2004, 2306–2307.

28 C. E. Fowler, D. Khushalani, B. Lebeau and S. Mann, *Adv. Mater.*, 2001, **13**, 649–652.

29 S. Sadasivan, C. E. Fowler, D. Khushalani and S. Mann, *Angew. Chem., Int. Ed.*, 2002, **41**, 2151–2153.

30 G. E. S. Toombes, S. Mahajan, M. Weyland, A. Jain, P. Du, M. Kamperman, S. M. Gruner, D. A. Muller and U. Wiesner, *Macromolecules*, 2008, **41**, 852–859.

31 M. Kruk and M. Jaroniec, *Chem. Mater.*, 2001, **13**, 3169–3183.

32 E. P. Barrett, L. G. Joyner and P. P. Halenda, *J. Am. Chem. Soc.*, 1951, **73**, 373–380.

33 R. Ryoo and J. M. Kim, *J. Chem. Soc., Chem. Commun.*, 1995, 711–712.

34 Q. S. Huo, D. I. Margolese, U. Ciesla, D. G. Demuth, P. Y. Feng, T. E. Gier, P. Sieger, A. Firouzi, B. F. Chmelka, F. Schuth and G. D. Stucky, *Chem. Mater.*, 1994, **6**, 1176–1191.

35 Q. S. Huo, D. I. Margolese, U. Ciesla, P. Y. Feng, T. E. Gier, P. Sieger, R. Leon, P. M. Petroff, F. Schuth and G. D. Stucky, *Nature*, 1994, **368**, 317–321.

36 R. I. Nooney, T. Dhanasekaran, Y. M. Chen, R. Josephs and A. E. Ostafin, *Adv. Mater.*, 2002, **14**, 529–532.

37 A. A. Chernov, D. E. Temkin and A. M. Mel'nikova, *Sov. Phys. Crystallogr. (Engl. Transl.)*, 1976, **21**, 369–374.

38 M. O. Kliya and I. G. Sokolova, *Sov. Phys. Crystallogr. (Engl. Transl.)*, 1958, **3**, 217–221.